s- and *d*-wave intruder strengths in $^{13}B_{g.s.}$ via the $^{1}H(^{13}B, d)^{12}B$ reaction

W. Liu,[1] J. L. Lou,[1,*] Y. L. Ye,[1] Z. H. Li,[1] Q. T. Li,[1] H. Hua,[1] X. F. Yang,[1] J. Y. Xu,[1] H. J. Ong,[2,3,4] D. T. Tran,[2,5] N. Aoi,[2] E. Ideguchi,[2] D. Y. Pang,[6] C. X. Yuan,[7] S. M. Wang,[8,9] Y. Jiang,[1] B. Yang,[1] Y. Liu,[1] J. G. Li,[1] Z. Q. Chen,[1] J. X. Han,[1] S. W. Bai,[1] G. Li,[1] K. Ma,[1] Z. W. Tan,[1] H. Y. Zhu,[1] and B. L. Xia[1]

[1]*School of Physics and State Key Laboratory of Nuclear Physics and Technology, Peking University, Beijing 100871, China*
[2]*Research Centre for Nuclear Physics, Osaka University, Ibaraki, Osaka 567-0047, Japan*
[3]*CAS Key Laboratory of High Precision Nuclear Spectroscopy, Institute of Modern Physics, Chinese Academy of Sciences, Lanzhou 730000, China*
[4]*School of Nuclear Science and Technology, University of Chinese Academy of Sciences, Beijing 100080, China*
[5]*Institute of Physics, Vietnam Academy of Science and Technology, Hanoi 10000, Vietnam*
[6]*School of Physics, Beijing Key Laboratory of Advanced Nuclear Materials and Physics, Beihang University, Beijing 100191, China*
[7]*Sino-French Institute of Nuclear Engineering and Technology, Sun Yat-Sen University, Zhuhai 519082, China*
[8]*Institute of Modern Physics, Fudan University, Shanghai 200433, China*
[9]*FRIB Laboratory, Michigan State University, East Lansing, Michigan 48824, USA*

(Received 26 February 2021; revised 22 October 2021; accepted 16 November 2021; published 8 December 2021)

Experimental results of the $^{1}H(^{13}B, d)^{12}B$ transfer reaction to the low-lying states in ^{12}B are reported. The optical potential parameters for the entrance channel are extracted from the elastic scattering $^{1}H(^{13}B, p)$ measured in the same experiment, while those for the exit channel are global ones. Spectroscopic factors associated with the *p*-, *s*-, and *d*-wave neutron transfer to the known ^{12}B states are extracted by comparing the deuteron angular distributions with the calculation results. The separated *s*- and *d*-wave intruder strengths in $^{13}B_{g.s.}$ were determined to be 5(2)% and 12(2)%, respectively, which follow roughly the systematics for the $N = 8$ neutron-rich isotones and shell model calculations with YSOX interaction. The sudden change of the intruder *sd*-wave intensity between ^{13}B and ^{12}Be needs further theoretical interpretation.

DOI: 10.1103/PhysRevC.104.064605

I. INTRODUCTION

Isospin dependence of nuclear structure and shell evolution is an interesting question of the finite Fermi system, which is composed of certain numbers of protons and neutrons [1]. For light stable nuclei with small N/Z asymmetry, the existence of the magic numbers can be well explained by the traditional shell model [2,3]. However, with increasing N/Z ratios, unusual rearrangements of single-particle orbitals emerge in the exotic nuclei far from the β-stability line [4–12].

For the ground state (g.s.) of stable $N = 8$ nuclei, the 0p0h configuration of $(1p_{1/2})^2_\nu$ is predominant according to the conventional shell model. However, the intruder 2p2h configurations of $(p_{1/2})^{-2}_\nu(2s_{1/2})^2_\nu$ (*s*-wave intruder) and $(p_{1/2})^{-2}_\nu(1d_{5/2})^2_\nu$ (*d*-wave intruder) have been widely investigated and reported for the neutron-rich $N = 8$ nuclei [5,6,8–10,13–15]. These kinds of intrusions can lead to the breakdown of the magic number $N = 8$. For the Borromean nucleus ^{11}Li, large *s*-wave intruder components in its g.s. (45%) [8] as well as in its low-lying excited states were observed [9,10], and were theoretically attributed to the effect of the tensor and pairing forces [16]. In the nucleus with one more proton, namely ^{12}Be, the *s*-wave component decreases to 19%, whereas the *d*-wave intrusion was found to be dominant [5]. The sudden increase of *d*-wave component in $^{12}Be_{g.s.}$ may be associated with the pairing interaction and deformation of the core [6]. For the nucleus with two more protons, namely ^{14}C, the g.s. is composed of only 1.3%-wave and slightly higher *d*-wave (8.4%) components, as obtained in a (p, d) transfer reaction [17], indicating the restoration of the $N = 8$ magic number. As a member of the $N = 8$ isotonic chain, between ^{12}Be and ^{14}C, ^{13}B offers an intriguing opportunity to systematically understand the neutron shell evolution as a function of proton number Z.

If we neglect the contributions from $1d_{3/2}$ and higher orbitals, and keep ^{11}B as the core, the wave function of $^{13}B_{g.s.}$ can be written as $|\text{g.s.}\rangle = \nu[a(1p_{1/2})^2 + b(2s_{1/2})^2 + c(1d_{5/2})^2]$, where a, b, and c stand for the spectroscopic amplitudes of *p*-, *s*-, and *d*-wave, respectively. *p* wave was found to be dominant in $^{13}B_{g.s.}$ based on the measurement of its magnetic dipole moment [18] and large *p*-wave spectroscopic factors (SFs) obtained from the knockout [19] and transfer [20] reactions. A 33% *s*-wave intruder strength in $^{13}B_{g.s.}$ was deduced from a ^{14}Be β-decay experiment, in which the emissions of β-delayed neutrons with very low energies from the 1^+_1 state were successfully measured [21]. In a charge-exchange reaction experiment of $^{13}C(t, {}^3He)\,^{13}B$ [22], the wave function of $^{13}B_{g.s.}$ was determined to be $|^{13}B\rangle_{g.s.} = 0.871\,|0\hbar\omega\rangle + 0.491\,|2\hbar\omega\rangle$, where $0\hbar\omega$ and $2\hbar\omega$ correspond

*jllou@pku.edu.cn

TABLE I. Neutron configurations in ^{12}B, calculated with shell model using the latest YSOX interaction [28].

Orbital	Spin-parity	Experiment	Shell model with YSOX					
		E_x (MeV)	$1p_{3/2}$	$1p_{1/2}$	$2s_{1/2}$	$1d_{5/2}$	$1d_{3/2}$	E_x (MeV)
$1p_{1/2}$	1^+_1	0.000	3.733	1.117	0.018	0.071	0.061	0.000
	2^+_1	0.953	3.861	1.016	0.011	0.052	0.060	1.395
$2s_{1/2}$	2^-_1	1.673	3.350	0.560	0.670	0.362	0.058	1.490
	1^-_1	2.621	3.361	0.556	0.847	0.175	0.061	2.222
$1d_{5/2}$	3^-_1	3.389	3.324	0.595	0.027	0.969	0.085	2.842
	2^-_2	4.460	3.319	0.624	0.200	0.784	0.074	3.359
	4^-_1	4.523	3.314	0.601	0.019	0.993	0.073	3.889
	1^-_3	6.000	3.324	0.602	0.058	0.778	0.238	5.688

to the normal p-wave and the intruder sd-wave components, respectively. This wave function gives a 24% intruder strength (a sum of s- and d-wave strengths), which is obviously smaller than the single s-wave intensity of 33% determined from the β-decay experiment, but is in good agreement with the shell model predictions from Fortune [23]. Therefore, it is necessary to further investigate s- and d-wave intruder intensities in ^{13}B$_{\text{g.s.}}$.

A single-neutron transfer reaction, which can selectively populate the states of interest, is a powerful probe to investigate the single-particle strengths of exotic nuclei [4]. In the present work, a ^{1}H(^{13}B, d) ^{12}B transfer reaction is adopted to populate the well-known low-lying states in ^{12}B. When a p-wave neutron is picked up by protons, the g.s. (1^+) and first excited state (2^+, 0.953 MeV) in ^{12}B will be populated. The ratio of SFs for these two states should be similar to that obtained from the one-neutron knockout reaction [19]. If a neutron in the $2s_{1/2}$ orbital is transferred, the coupling of a residual $2s_{1/2}$ neutron with a $1p_{3/2}$ proton would lead to $(2, 1)^-$ doublet at 1.674 and 2.621 MeV. With a $1d_{5/2}$ neutron transferred, the configuration of $(1p_{3/2})^1_\pi \otimes (1d_{5/2})^1_\nu$ gives the 3^-_1 (3.389 MeV), 2^-_2 (4.406 MeV), 4^-_1 (4.523 MeV), and 1^-_3 (6.000 MeV) states according to the experimental data [20,24–27] and the shell model calculations with the latest YSOX interaction [28], which are shown in Table I. The single-particle properties of the states in ^{12}B mentioned above have been studied through several different ^{2}H(^{11}B, p) ^{12}B reactions [20,24,25]. Therefore, the population of negative-parity states in ^{12}B via the ^{1}H(^{13}B, d) ^{12}B reaction will provide direct evidence for the s- and d-wave intrusions in ^{13}B$_{\text{g.s.}}$.

In this paper, the experimental results of the first ^{1}H(^{13}B, d) ^{12}B transfer reaction using a radioactive beam of ^{13}B at 23 MeV/nucleon are presented. The experimental setup and results of the reactions on the polyethylene target are described in Secs. II and III, respectively. A brief summary is given in Sec. IV.

II. EXPERIMENTAL DETAILS

The experiment was performed at the EN-course beam line at Research Center for Nuclear Physics (RCNP), Osaka University [29,30]. A 23-MeV/nucleon ^{13}B secondary beam was produced from a 58-MeV/nucleon ^{18}O primary beam impinging on a 3.8-mm-thick ^{9}Be target. The secondary beam was purified by the electromagnetic separator after punching through a 3.07- mm-thick aluminium degrader. The beam purity and intensity were 98% and $\sim 2.0 \times 10^4$ particles per second, respectively. The momentum spread was limited, by a slit, down to $\Delta p/p \leqslant 0.75\%$ to reduce the energy dispersion of the secondary beam.

The experimental setup is schematically shown in Fig. 1. The secondary beam was identified by the time of flight (TOF), which was provided by two plastic scintillation detectors (F2 plastic and F3 plastic), and energy losses in F3 plastic. Two x-y position-sensitive parallel plate avalanche chambers (PPACs) were employed to track the ^{13}B beam before the physical target. The position resolution of two PPACs was about 1.5 mm [full width at half maximum (FWHM)], and the distance between them was about 772 mm. A 6.76-mg/cm^2 polyethylene target $(CH_2)_n$ and a 3.98-mg/cm^2 deuterated polyethylene target $(CD_2)_n$ were installed. Both targets were rotated 20 $^\circ$ with respect to the beam direction in order to reduce the energy losses in the target of the low-energy charged particles emitting to the telescopes T2 and T1 (as shown in Fig. 1).

Four sets of charged-particle telescopes (T0, T1, T2, TA) were employed in the large scattering chamber, as shown in Fig. 1. T0, T1, and T2 were used to detect the residual nuclei around the beam direction, the reaction-produced light particles, and the elastically scattered protons and deuterons at large angles, respectively. TA was placed at backward angles to detect the protons from the ^{2}H(^{13}B, p) ^{14}B reaction.

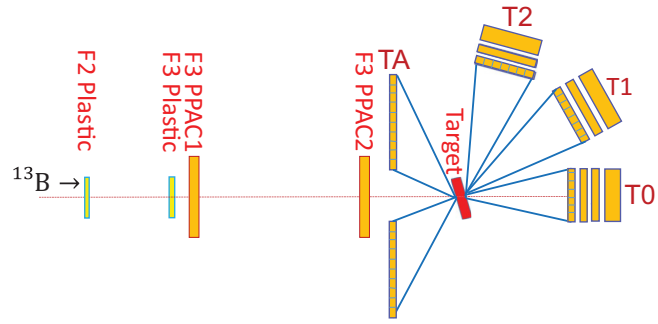

FIG. 1. Schematic view of the experimental setup.

T0, consisting of a double-sided silicon strip (DSSD) detector with a thickness of 1000 μm, two large size silicon detectors (SSDs), and a layer of 4-cm-thick CsI(Tl) crystals read out by photodiodes, was centered at 0° with respect to the beam direction. T2, which was composed of a 60-mm-thick DSSD and a SSD, was installed around 70° with respect to the beam direction. An array of 4-cm-thick CsI(Tl) crystals was placed behind SSD to stop high energy particles. T1 was placed around 31°, with the same composition as T2. Each DSSD used in these three sets of telescopes was divided into 32 strips on both sides and had an active area of 64×64 mm^2. Each SSD had the same active size as the DSSDs while its nominal thickness was 1500 μm. TA is a set of the annular double-sided silicon strip detector (ADSSD) composed of six sectors. The distances between the center of target and the first layer of each telescope were 200, 150, 150, and 190 mm for T0, T1, T2, and TA, respectively.

GEANT4 simulation [31] was performed to estimate the angular resolution and the possible angular shift of each telescope. The angular resolution of the telescopes T2 (and T1) approximates 0.9° (FWHM), taking into consideration the uncertainty of hitting position on the target (1.5 mm) determining from the PPACs and the strip width of DSSD (2 mm). Considering the machining accuracy (0.5 mm) of frames and the uncertainty in position calibration (0.25 mm), the possible angular shift is smaller than 0.3°. The energy resolution of the silicon detectors was less than 1% for α particles at 5.486 MeV, which was sufficient to discriminate the nuclei lighter than carbon, with the standard $\Delta E - E$ method.

In this paper, we will focus on the (p, p) elastic scattering and (p, d) transfer reaction between ^{13}B and the $(CH_2)_n$ target. The light particles detected in T2 or T1 are analyzed in coincidence with the residual nuclei detected in T0. Data from the coincidence of T0 and TA are not involved in this paper.

III. RESULTS

A. Particle identification

The experiment was performed in inverse kinematics, and different reaction channels were discriminated by the coincidence of boron isotopes detected by T0 and light particles measured by the other telescopes. As shown in Fig. 2, protons detected in T2 are clearly identified. They are mainly from the elastic/inelastic scattering of ^{13}B on the $(CH_2)_n$ target. The inset of Fig. 2 shows the particle identification (PID) spectrum detected in T0 after gated on the protons detected in T2, in which ^{13}B is predominant.

Figure 3 displays the boron isotopes detected in T0, with the gate of light particles measured in T1. The hydrogen isotopes detected in T1 are shown in the inset of Fig. 3. The neutron threshold of ^{12}B is $S_n = 3.370$ MeV. For the excited states above this threshold, the produced ^{12}B can decay to ^{11}B by emitting one neutron. Normally, ^{12}B and ^{11}B can be seen and separated from ^{13}B in T0, which is similar to the results in [32]. ^{11}B, ^{12}B, and ^{13}B are clearly seen, but are not separated well due to the poor energy resolution of the first layer SSD in T0. The analysis of cross section in the following subsections was based on the coincidence of light charged particles in T1 or T2, and boron isotopes in Fig. 3 or the inset of Fig. 2.

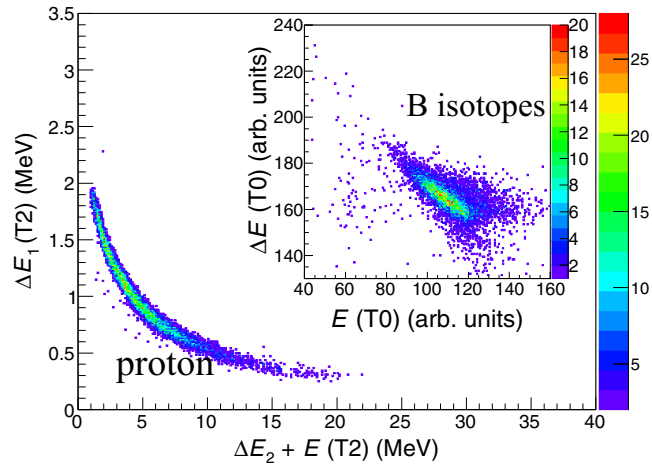

FIG. 2. Protons elastically scattered from ^{13}B in the particle identification (PID) spectrum measured by T2. The inset figure shows the PID spectrum measured by T0, where the Boron isotopes are shown in coincidence with protons.

B. Elastic scattering

Figure 4 exhibits the proton energies as a function of outgoing angles. Most events are consistent with the calculated kinematic curve of elastic scattering (red solid curve). Figure 5 displays the excitation energy spectrum of ^{13}B, which is deduced from the energies and angles of protons detected in T2. The center of the elastic scattering peak is zero. Its resolution of 776 keV (FWHM) is in good agreement with the simulated result using the code GEANT4 [31], taking into consideration the real experimental setup.

A few inelastic scattering events appear in Fig. 4. As shown in the inset of Fig. 5, the excitation energy spectrum of ^{13}B, a wide peak at around 3–5 MeV is observed. This peak mainly corresponds to the first and the second positive-parity excited

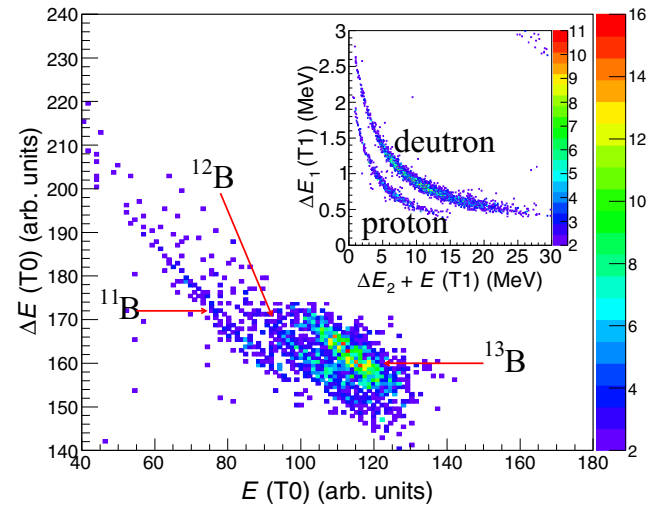

FIG. 3. The PID spectrum of boron isotopes detected by T0 in coincidence with T1. The inset shows the PID spectrum measured by T1.

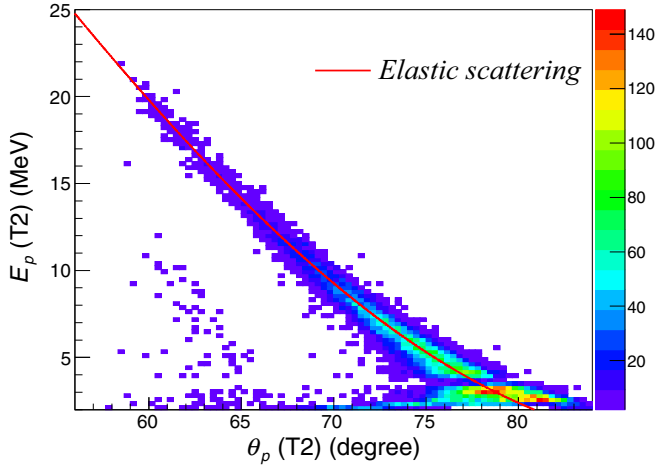

FIG. 4. Bi-dimensional plot of energy vs angle for recoiling protons in coincidence with ^{13}B at forward angles. The red solid curve stands for the kinematic loci of the elastic scattering.

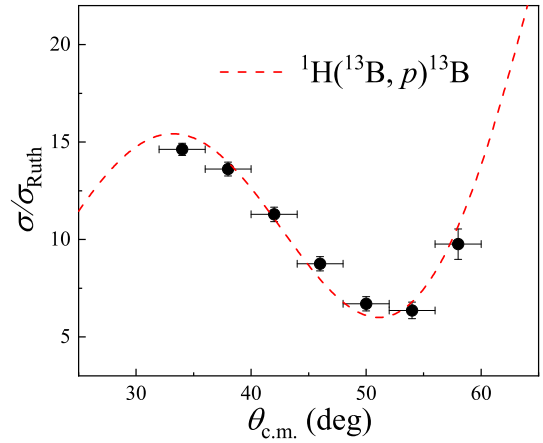

FIG. 6. Elastic scattering differential cross sections, relative to the Rutherford cross sections. Theoretical calculations using the normalized WSS potential (red dashed curve) reproduce the experimental data. See text for more details.

states of ^{13}B at 3.48 and 3.68 MeV, which are formed by the excitation of one neutron from the $1p_{1/2}$ orbital to the $2s_{1/2}$ and the $1d_{5/2}$ orbital [24], respectively. Due to the limited acceptance of T2, higher excited states in ^{13}B are not observed.

The elastic scattering differential cross sections, as a ratio to the Rutherford cross sections, are shown in Fig. 6. The count for each point, which corresponds to an angular range of 2° in the laboratory frame, is obtained by fitting the peak at around 0 in the excitation energy spectrum of ^{13}B (Fig. 5). A Gaussian peak with the simulated width was used to fit the spectrum. Only the amplitude of the Gaussian function was left as a free parameter for each point. The error bars are purely statistical. The systematic error is less than 9%, considering the uncertainties in the geometrical efficiency determination, the thickness of the target, and the cuts on the PID spectra (Fig. 2).

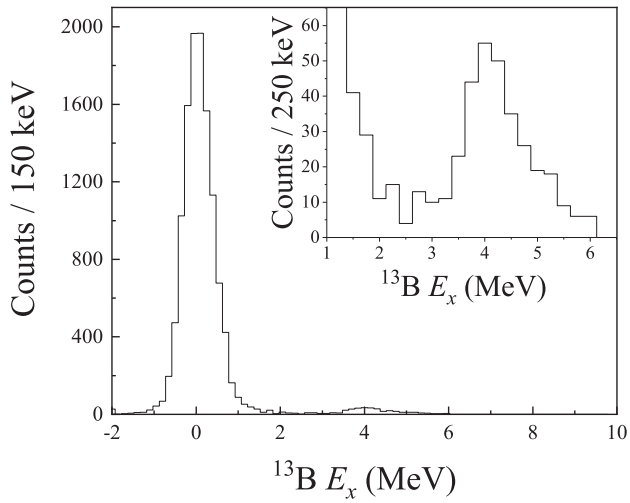

FIG. 5. Excitation energy spectrum of ^{13}B reconstructed from the energies and angles of the scattered protons measured by T2. The inset figure shows the energy spectrum for inelastic scattering.

The optical model is a powerful tool to describe the elastic scattering [33]. Three sets of global optical potentials (OPs), CH89 [34], KD02 [35], and WSS [36], were tried in the calculations with the code FRESCO [37] to reproduce the elastic scattering angular distributions. To better reproduce the experimental data, two normalization factors, λ_V and λ_W, were introduced to the depths of the real (V_V) and the imaginary part ($W_V + W_S$), respectively [38]. The geometric parameters r_0 and a were adopted the same as those of the global OPs. The searching process for the renormalization factors was based on the χ^2 minimization method. As shown in Fig. 6, the normalized WSS potential provides a good reproduction of the current data. The best optical potential parameters are listed in Table II.

C. ^{1}H(^{13}B, d)^{12}B transfer reaction

In coincidence with boron isotopes, the bidimensional spectrum for the deuteron energies as a function of outgoing angles is given in Fig. 7. Most events agree with the calculated kinematics of the ^{1}H(^{13}B, d)^{12}B transfer reaction to the states of interest in ^{12}B. The excitation energy spectra of ^{12}B presented in Fig. 8 were reconstructed from the energies and angles of deuterons emitting to different angular ranges in coincidence with boron isotopes measured by T0. The spectra were fitted with nine known states of ^{12}B, namely the g.s. and the excited states at E_x = 0.953, 1.674, 2.723, 3.389, 3.760, 4.523, 4.990, and 5.610 MeV. Monte Carlo simulations were performed to estimate the resolution as a function of the excitation energy in the laboratory frame, taking into consideration the beam profile, the beam energy spread (1.5%), the uncertainty of target thickness, the energy threshold (0.3 MeV) of the silicon strip detectors, energy losses of deuterons/protons in the target and in the dead layers of silicon detectors, and the geometry of T0 and T1/T2, and so on [38]. An integrated energy resolution of about 0.73–0.55 MeV (FWHM) was obtained for the states in the excitation energy range E_x = 0.0–6.0 MeV. All the states

TABLE II. Parameters of the optical model potentials for the elastic scattering and ^{1}H(^{13}B, d) ^{12}B reaction calculations.

Channel	V_0 (MeV)	r_0 (fm)	a_0 (fm)	W (MeV)	r_W (fm)	a_W (fm)	W_D (MeV · fm)	r_{W_D} (fm)	a_{W_D} (fm)	$V_{\text{s.o.}}$ (fm)	$r_{\text{s.o.}}$ (fm)	$a_{\text{s.o.}}$ (fm)	r_C (fm)
^{13}B + p	64.516	1.128	0.570	0.000			10.798	1.128	0.500	5.500	1.128	0.570	1.128
^{12}B + d	83.948	1.170	0.751	0.772	1.325	0.659	12.075	1.325	0.659	3.304	1.070	0.660	1.300
^{12}B + p	58.921	1.128	0.570	0.000			9.976	1.128	0.500	5.500	1.128	0.570	1.128

were fitted with Gaussian functions, except for the 5.610-MeV state with a large intrinsic width (110 keV [39]). The peak position for each peak was fixed at the well-known excitation energy. The widths were set to the simulated resolution values. Only the amplitudes were left as free parameters. Considering a large intrinsic width of the 5.610-MeV state, a Breit-Wigner function convoluted with the simulated resolution of the detector system was adopted [9]. In this experiment, both the energy and the time information of each detector were recorded. A time cut was used when analyzing the excitation energy spectra from the coincidence events. The background contributions from reactions with carbon in the physical target of $(CH_2)_n$ were negligible, which were verified by the analysis with the carbon and the empty target. Thus, no background was included in the fitting functions. Considering the limited statistics, the maximum likelihood method described in Ref. [40] was used to search for the best fitting parameters.

Differential cross sections for the populated states of interest are depicted in Fig. 9. The error bars are purely statistical. The systematic error is less than 11%, taking into consideration the uncertainties in the geometrical efficiency determination, the thickness of the target, and the cuts of deuterons and borons on the PID spectra.

To extract the SFs, the distorted wave Born approximation (DWBA) calculation was performed with the code FRESCO [37]. The normalized WSS potential parameters extracted from the elastic scattering angular distributions were adopted for the entrance channel. The systematic optical potential of Daehnick *et al.* [41] was used for the exit channel. The Reid soft-core potential [42] was employed to reproduce the binding energy of deuteron. For the interaction between ^{12}B and a neutron, the Woods-Saxon potential was chosen. The geometry parameters r_0 and a were set to 1.25 and 0.65 fm, respectively. The depths of binding potentials were adjusted to reproduce the binding energy of ^{13}B. As shown in Fig. 9, the red dashed curves are the calculated differential cross sections for each state, which have been multiplied by the corresponding SFs extracted in this experiment. Note that the doublet formed by the transfer of the $1d_{5/2}$ neutron, namely the 4.406- and 4.523-MeV states, is not resolved due to the limited Q-value resolution. Considering the limited statistics of the differential cross sections for this doublet [as shown in Fig. 9(f)], it is difficult to decompose it by using two components. The lower and upper limit of the SF were extracted by comparing the differential cross sections to the theoretical ones calculated for the 4.406- and 4.523-MeV states, respectively. The statistics at the 6.00-MeV state are too low to extract differential cross sections due to rapid decreasing detection efficiency. The d-wave SF of the 6.00-MeV state was smaller than 0.01 based on the shell model predictions; see Table III.

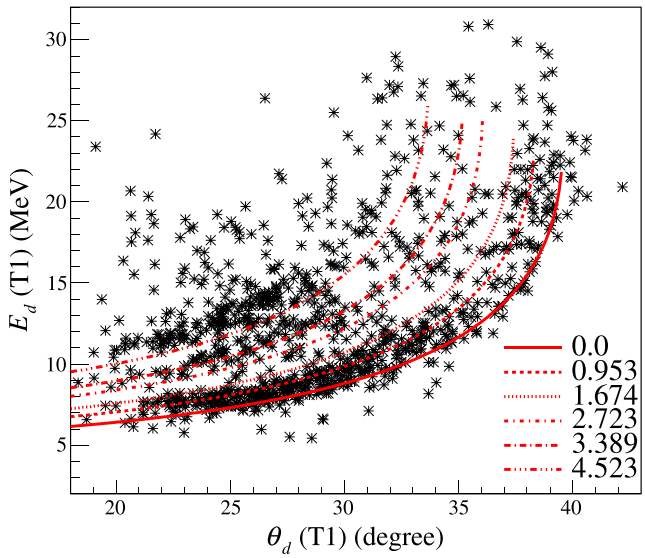

FIG. 7. The deuteron energies versus outgoing angles in laboratory frame, gated on the boron isotopes measured by T0. The red lines stand for the calculated kinematics of the ^{1}H(^{13}B, d) ^{12}B transfer reaction to the states of interests in ^{12}B.

Since the experimental SFs are sensitive to the choice of OPs and practical experimental conditions [4,5], the relative SFs are more meaningful. According to the sum rule [43], the sum of all the p-, s-, and d-wave SFs, corresponding to the $l = 1$, 0, and 2 neutron transfer in the ^{1}H(^{13}B$_{\text{g.s.}}$, d) reaction, should be equal to 2.0. Based on this principle, the experimental SFs for single-particle states formed by p-, s-, and d-wave neutron were normalized to obtain the relative SFs, and the results are summarized in Table III. The uncertainties of the SFs correspond to a 68% confidence level with $\chi^2_{\text{min}} + 1$ except for the 2.6212-MeV state. The SF uncertainty of the 2.621-MeV state was deduced from $\chi^2_{\text{min}} + 2.3$, because two parameters were used in the fit to the corresponding differential cross sections. The ratio of SFs for the g.s. and first excited state is in agreement with that obtained from the single-neutron knockout reaction [19].

We found that the s-wave SFs largely depend on the amplitude at surface region and the assumed binding energy. If we used a binding energy of 4.12 MeV (half of two neutron binding energy of ^{13}B) for the 1.674-MeV state, the calculated cross sections increased obviously, leading to an s-wave SF of 0.04(1) for the 1.674-MeV state (lower limit). Finally, the s-wave SF for this state was determined to be 0.06(2).

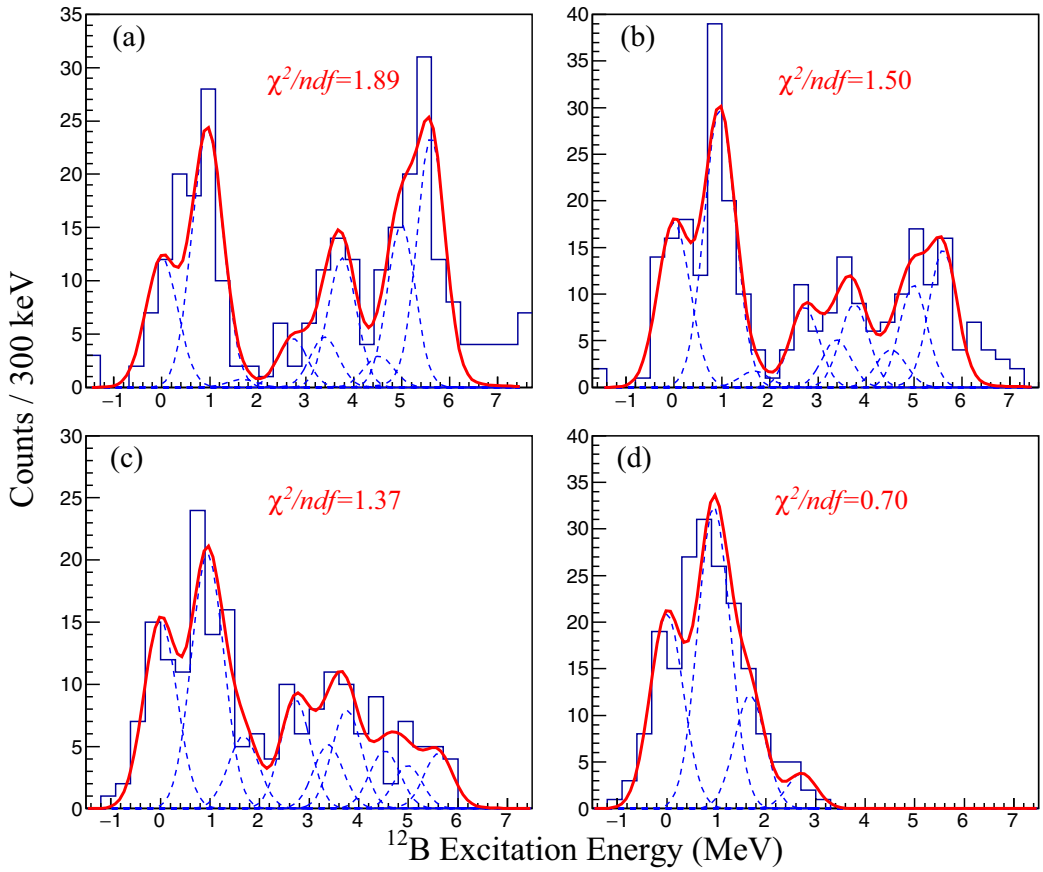

FIG. 8. Excitation energy spectra of ^{12}B reconstructed from the energies and angles of deuterons at (a) 23–27°, (b) 27–31°, (c) 31–35°, and (d) 35–39°. The blue solid lines show the fitted spectrum for each state, and the red solid curves show the total fits, i.e., sums of blue solid curves. Note that the amplitudes for states above 3 MeV are zero in (d). The number of degrees of freedom (ndf) corresponds to the number of points used in the fit minus the number of free parameters.

D. *s*- and *d*-wave strengths in ^{13}B$_{g.s.}$

By ignoring the contributions from $1d_{3/2}$ and higher orbitals, the g.s. of ^{13}B could be written as $|\text{g.s.}\rangle = \nu[a(1p_{1/2})^2 + b(2s_{1/2})^2 + c(1d_{5/2})^2]$, with the normalization relation of $a^2 + b^2 + c^2 = \alpha + \beta + \gamma = 1$, where α, β, and γ are the *p*-, *s*-, and *d*-wave intensities, respectively. The ratio

TABLE III. Excitation energies and SFs for the low-lying states in ^{12}B. The relative SFs are extracted from the present ^{1}H(^{13}B, *d*) reaction to the lowing-lying states in ^{12}B and the corresponding uncertainties are from the fit to the differential cross sections for each state based on the χ^2 minimization method. Comparing with the experimental results, the shell model calculation results with the WBP [44] interaction and the latest YSOX interaction [28] are also listed.

Spin-parity	Orbital	Expt.		YSOX		WBP	
		E_x (MeV)	SF$_{rel}$	E_x (MeV)	SF	E_x (MeV)	SF
1^+_1	$1p_{1/2}$	0.000	0.54(5)	0.000	0.49	0.000	0.53
2^+_1	$1p_{1/2}$	0.953	1.11(7)	1.395	0.96	1.631	1.04
2^-_1	$2s_{1/2}$	1.674	0.06(2)[a]	1.490	0.04	2.885	0.003
1^-_1	$2s_{1/2}$	2.621	0.04(1)	2.222	0.02	3.702	0.003
3^-_1	$1d_{5/2}$	3.389	0.13(2)	2.842	0.10	4.193	0.03
2^-_2	$1d_{5/2}$	4.460	0.11(2)[b]	3.359	0.03	4.362	0.006
4^-_1	$1d_{5/2}$	4.523		3.889	0.06	4.348	0.02
1^-_3	$1d_{5/2}$	6.000	<0.01[c]	5.688	<0.01	6.464	<0.01

[a]Besides statistic errors, the effect of the binding energy was also considered. See text for more details.
[b]Sum of the SFs of the 4.460- and 4.523-MeV states, see text for more details.
[c]Not observed. Calculated with YSOX interaction.

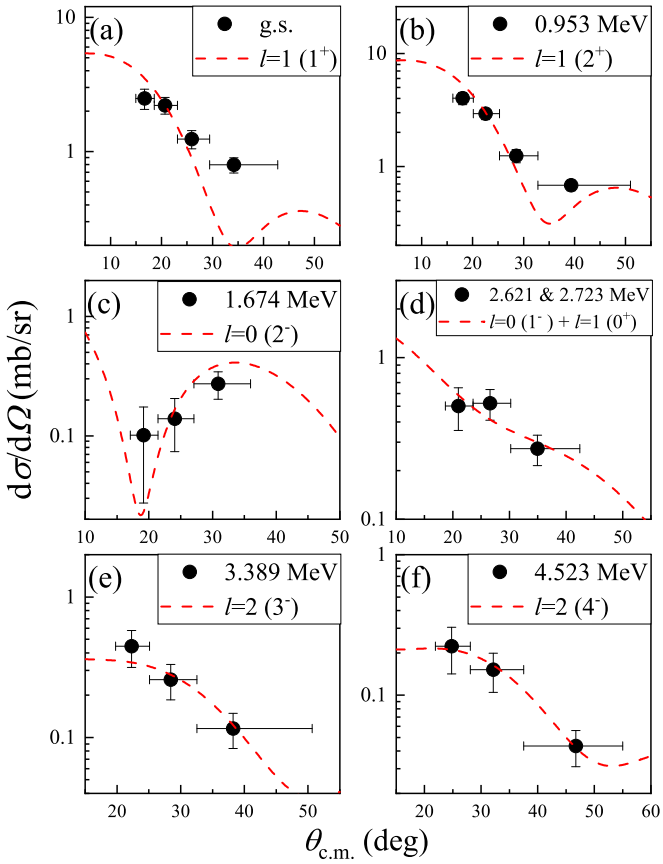

FIG. 9. Differential cross sections of ^{1}H(^{13}B, d) to the excited states at (a) 0.00, (b) 0.953, (c) 1.674, (d) 2.261 and 2.723, (e) 3.389, (f) 4.523 MeV. The excitation energy, the spin parity, and the transferred orbital angular momentum l, are given in the figure. The red dashed curves are the calculated differential cross sections for each state, multiplied by the corresponding SFs. The 2.621-MeV state could not be separated from the 2.723-MeV state in this experiment, so it was fitted as one peak in Fig. 8 and decomposed by two components in (d).

of α, β, and γ is deduced from the relative SFs of low-lying states in ^{12}B populated by the transfer of the p-, s-, and d-wave neutron in the present ^{1}H(^{13}B, d) ^{12}B reaction. Based on the studies of ^{14}C$_{g.s.}$ via (p, d) transfer reaction [17,45], contributions of p-, s-, and d-wave strengths from high-lying excited states are small and can be ignored. Combining the ratio of α, β with γ and $\alpha + \beta + \gamma = 1$, we obtained $\alpha = 83(6)\%$, $\beta = 5(2)\%$, and $\gamma = 12(2)\%$. The intruder s-wave intensity of 5(2)% extracted directly from our experiment is dramatically lower than 33%, which was indirectly deduced from the ^{14}Be β-decay experiment [21]. However, the sum of intruder s- and d-wave strength is 17(3)%, which is close to 24% obtained from the charge-exchange reaction [22].

Figure 10(a) shows the experimental results of the p-, s-, and d-wave intensities in ^{12}Be$_{g.s.}$ [5], ^{13}B$_{g.s.}$, and ^{14}C$_{g.s.}$ [17]. It can be seen that the results of ^{13}B$_{g.s.}$ are consistent with the systematical trends of the $N = 8$ isotones. The intensity of the p wave increases with increasing Z value, whereas the intensities of the intruder s- and d-wave decrease dramatically. With difference of merely one proton, the s-/d-wave intruder

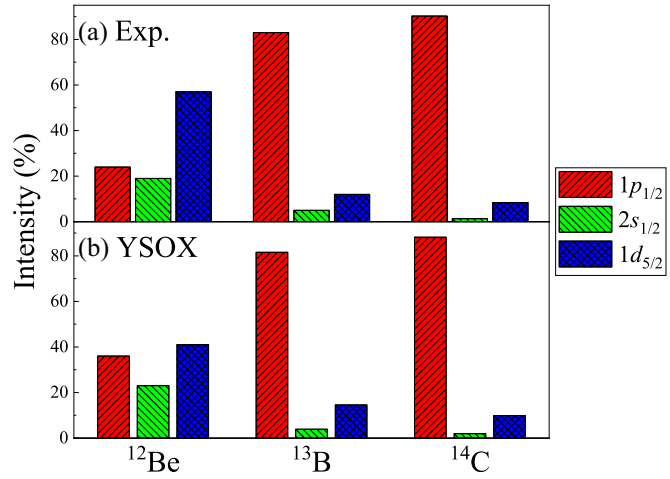

FIG. 10. (a) Individual p-, s-, and d-wave intensities in the ground state of ^{12}Be [5], ^{13}B (this work), and ^{14}C [17]. (b) Shell model calculations with YSOX interaction in full p-sd model space. The results for ^{12}Be are from Ref. [5].

strength changes suddenly from ^{12}Be to ^{13}B, but remains nearly a constant from ^{13}B to ^{14}C. The sudden change of the intruder configuration between ^{12}Be and ^{13}B is interesting and needs further theoretical interpretation.

In comparison with the experimental results, the p-, s-, and d-wave intensities calculated from the shell model with the YSOX interaction [28] are demonstrated in Fig. 10(b). The calculations were performed in a full p-sd model space. The measured s-, d-, and p-wave intensities for these nuclei can be fairly reproduced by the calculations. The total sd-wave intruder strength of 17(3)% from this experiment is in good agreement with 15% from the shell model calculation.

We also performed calculations within the Gamow coupled-channel (GCC) approach by assuming ^{13}B as a deformed ^{11}B core plus two neutrons, together with coupling to the continuum. The calculation adopted the same interaction and model space as in Ref. [46], which has successfully reproduced the low-lying excited states in ^{12}Be. As a result, the calculated intruder s- and d-wave strengths in ^{13}B$_{g.s.}$ are only 2.06% and 2.35%, respectively, by treating the valence proton as a speculator. If we considered the effect of pn interaction, the total intruder strength would even decrease to less than 2%. For ^{12}Be$_{g.s.}$, the calculated d-wave intensity of 25% is only half of the experimental data, while the s-wave strength of 20% is nearly the same as the measured value [46]. This implies different structures in ^{13}B and ^{12}Be, particularly the restoration of $N = 8$ magic shell. In order to better reproduce the experimental results, the strength of nucleon-nucleon interaction could vary in different nuclear mediums.

IV. SUMMARY

In summary, the ^{1}H(^{13}B, d) ^{12}B transfer reaction was performed with a 23-MeV/nucleon ^{13}B beam. With the optical potential extracted from the elastic scattering data measured in the same experiment, the relative SFs associated with the ^{13}B$_{g.s.}$ configuration were determined through the

measurements of a single-neutron transfer reaction to the known ^{12}B states. The *s*- and *d*-wave intruder strengths in $^{13}B_{g.s.}$ are deduced quantitatively, which are consistent with the systematics of $N = 8$ neutron-rich isotones and shell model calculations. The total intruder 2p2h strength including both *s*- and *d*-wave is in good agreement with the shell model calculations. However, the sudden increase of the intruder *sd*-wave intensity moving from $^{13}B_{g.s.}$ to $^{12}Be_{g.s.}$ needs further theoretical interpretation. The present work demonstrates that the single-nucleon transfer reaction in inverse kinematics is a sensitive tool to investigate the configuration mixing, including the intruder phenomena, in unstable neutron-rich nuclei.

ACKNOWLEDGMENTS

We gratefully thank the RCNP accelerator group for providing ^{18}O primary beam and the RCNP technical staff for assistance. This work was supported by the National Key R&D Program of China (Grant No. 2018YFA0404403), the National Natural Science Foundation of China (Contracts No. 11775004, No. U1867214, No. 11775013, No. 11775316, No. 11875074, No. 11961141003, and No. U2067205), and the funding from the State Key Laboratory of Nuclear Physics and Technology, Peking University (No. NPT2021ZZ01).

[1] T. Otsuka, A. Gade, O. Sorlin, T. Suzuki, and Y. Utsuno, Rev. Mod. Phys. **92**, 015002 (2020).
[2] M. G. Mayer, Phys. Rev. **75**, 1969 (1949).
[3] O. Haxel, J. H. D. Jensen, and H. E. Suess, Phys. Rev. **75**, 1766 (1949).
[4] W. Liu, J. L. Lou, Y. L. Ye, and D. Y. Pang, Nucl. Sci. Tech. **31**, 20 (2020).
[5] J. Chen, J. L. Lou, Y. L. Ye, Z. H. Li, D. Y. Pang, C. X. Yuan, Y. C. Ge, Q. T. Li, H. Hua, D. X. Jiang *et al.*, Phys. Lett. B **781**, 412 (2018).
[6] J. Chen, J. L. Lou, Y. L. Ye, Z. H. Li, D. Y. Pang, C. X. Yuan, Y. C. Ge, Q. T. Li, H. Hua, D. X. Jiang, X. F. Yang, F. R. Xu, J. C. Pei, J. Li, W. Jiang, Y. L. Sun, H. L. Zang, Y. Zhang, G. Li, N. Aoi *et al.*, Phys. Rev. C **98**, 014616 (2018).
[7] J. Chen, S. M. Wang, H. T. Fortune, J. L. Lou, Y. L. Ye, Z. H. Li, N. Michel, J. G. Li, C. X. Yuan, Y. C. Ge, Q. T. Li, H. Hua, D. X. Jiang, X. F. Yang, D. Y. Pang, F. R. Xu, W. Zuo, J. C. Pei, J. Li, W. Jiang *et al.*, Phys. Rev. C **103**, L031302 (2021).
[8] I. Tanihata, M. Alcorta, D. Bandyopadhyay, R. Bieri, L. Buchmann, B. Davids, N. Galinski, D. Howell, W. Mills, S. Mythili, R. Openshaw, E. Padilla-Rodal, G. Ruprecht, G. Shiffer, A. C. Shotter, M. Trinczek, P. Walden, H. Savajols, T. Roger, M. Caamano *et al.*, Phys. Rev. Lett. **100**, 192502 (2008).
[9] J. Tanaka, R. Kanungo, M. Alcorta, N. Aoi, H. Bidaman, C. Burbadge *et al.*, Phys. Lett. B **774**, 268 (2017).
[10] R. Kanungo, A. Sanetullaev, J. Tanaka, S. Ishimoto, G. Hagen, T. Myo, T. Suzuki, C. Andreoiu, P. Bender, A. A. Chen, B. Davids, J. Fallis, J. P. Fortin, N. Galinski, A. T. Gallant, P. E. Garrett, G. Hackman, B. Hadinia, G. Jansen, M. Keefe *et al.*, Phys. Rev. Lett. **114**, 192502 (2015).
[11] C. R. Hoffman, B. P. Kay, and J. P. Schiffer, Phys. Rev. C **89**, 061305(R) (2014).
[12] C. R. Hoffman, B. P. Kay, and J. P. Schiffer, Phys. Rev. C **94**, 024330 (2016).
[13] H. Iwasaki, A. Dewald, C. Fransen, A. Gelberg, M. Hackstein, J. Jolie, P. Petkov, T. Pissulla, W. Rother, and K. O. Zell *et al.*, Phys. Rev. Lett. **102**, 202502 (2009).
[14] D. T. Tran, H. J. Ong, G. Hagen, T. D. Morris, N. Aoi, T. Suzuki *et al.*, Nat. Commun. **9**, 1594 (2018).
[15] S. Ota, S. Shimoura, H. Iwasaki, M. Kurokawa, S. Michimasa, N. Aoi *et al.*, Phys. Lett. B **666**, 311 (2008).
[16] T. Myo, K. Kato, H. Toki, and K. Ikeda, Phys. Rev. C **76**, 024305 (2007).
[17] F. Cecil, J. Shepard, R. Anderson, R. Peterson, and P. Kaczkowski, Nucl. Phys. A **255**, 243 (1975).
[18] R. L. Williams and L. Madansky, Phys. Rev. C **3**, 2149 (1971).
[19] E. Sauvan, F. Carstoiu, N. A. Orr, J. S. Winfield, M. Freer, J. C. Angelique, W. N. Catford, N. M. Clarke, M. MacCormick, N. Curtis, S. Grevy, C. LeBrun, M. Lewitowicz, E. Liegard, F. M. Marques, P. Roussel-Chomaz, M. G. SaintLaurent, and M. Shawcross, Phys. Rev. C **69**, 044603 (2004).
[20] H. Y. Lee, J. P. Greene, C. L. Jiang, R. C. Pardo, K. E. Rehm, J. P. Schiffer, A. H. Wuosmaa, N. J. Goodman, J. C. Lighthall, S. T. Marley, K. Otsuki, N. Patel, M. Beard, M. Notani, and X. D. Tang, Phys. Rev. C **81**, 015802 (2010).
[21] N. Aoi, K. Yoneda, E. Ideguchi, T. Kishida, T. Nakamura, M. Notani, H. Sakurai, T. Teranishi, Y. Watanabe, H. Wu, A. Yoshida, H. Miyatake, Y. Yamamoto, H. Ogawa, S. S. Yamamoto, and M. Ishihara, Phys. Rev. C **66**, 014301 (2002).
[22] C. J. Guess, R. G. T. Zegers, B. A. Brown, S. M. Austin, D. Bazin, C. Caesar, J. M. Deaven, G. F. Grinyer, C. Herlitzius, G. W. Hitt, S. Noji, R. Meharchand, G. Perdikakis, H. Sakai, Y. Shimbara, and C. Tur, Phys. Rev. C **80**, 024305 (2009).
[23] H. T. Fortune and R. Sherr, Phys. Rev. C **68**, 024301 (2003).
[24] B. B. Back, S. I. Baker, B. A. Brown, C. M. Deibel, S. J. Freeman, B. J. DiGiovine, C. R. Hoffman, B. P. Kay, H. Y. Lee, J. C. Lighthall, S. T. Marley, R. C. Pardo, K. E. Rehm, J. P. Schiffer, D. V. Shetty, A. W. Vann, J. Winkelbauer, and A. H. Wuosmaa, Phys. Rev. Lett. **104**, 132501 (2010).
[25] T. L. Belyaeva, S. A. Goncharov, A. S. Demyanova, A. A. Ogloblin, A. N. Danilov, V. A. Maslov, Y. G. Sobolev, W. Trzaska, S. V. Khlebnikov, G. P. Tyurin, N. Burtebaev, D. Janseitov, and E. Mukhamejanov, Phys. Rev. C **98**, 034602 (2018).
[26] P. Koehler, H. Knox, D. Resler, R. Lane, and D. Millener, Nucl. Phys. A **394**, 221 (1983).
[27] J. Kelley, J. Purcell, and C. Sheu, Nucl. Phys. A **968**, 71 (2017).
[28] C. Yuan, T. Suzuki, T. Otsuka, F. Xu, and N. Tsunoda, Phys. Rev. C **85**, 064324 (2012).
[29] T. Shimoda, H. Miyatake, and S. Morinobu, Nucl. Instrum. Methods Phys. Res. B **70**, 320 (1992).
[30] H. J. Ong, in *Frontiers in Physics: 4th International Meeting*, edited by K. Ratnavelu, S.-P. Chia, C. S. Wong, and R. Chong-Heng Ooi, AIP Proc. No. 1588 (AIP, Melville, NY, 2014), pp. 146–150.
[31] S. Agostinelli, J. Allison, K. Amako, J. Apostolakis, H. Araujo, P. Arce *et al.*, Nucl. Instrum. Methods Phys. Res. A **506**, 250 (2003).
[32] Y. Jiang, J. L. Lou, Y. L. Ye, D. Y. Pang, J. Chen, Z. H. Li *et al.*, Chin. Phys. Lett. **35**, 082501 (2018).

[33] W. Dickhoff and R. Charity, Prog. Part. Nucl. Phys. **105**, 252 (2019).
[34] R. Varner, W. Thompson, T. McAbee, E. Ludwig, and T. Clegg, Phys. Rep. **201**, 57 (1991).
[35] A. Koning and J. Delaroche, Nucl. Phys. A **713**, 231 (2003).
[36] B. A. Watson, P. P. Singh, and R. E. Segel, Phys. Rev. **182**, 977 (1969).
[37] I. J. Thompson, Comput. Phys. Rep. **7**, 167 (1988).
[38] J. Chen, J. L. Lou, Y. L. Ye, Z. H. Li, Y. C. Ge, Q. T. Li, J. Li, W. Jiang, Y. L. Sun, H. L. Zang, N. Aoi, E. Ideguchi, H. J. Ong, Y. Ayyad, K. Hatanaka, D. T. Tran, T. Yamamoto, M. Tanaka, T. Suzuki, N. T. Tho *et al.*, Phys. Rev. C **93**, 034623 (2016).
[39] F. Ajzenberg-Selove, Nucl. Phys. A **506**, 1 (1990).
[40] S. Baker and R. D. Cousins, Nucl. Instrum. Methods Phys. Res. A **221**, 437 (1984).
[41] W. W. Daehnick, J. D. Childs, and Z. Vrcelj, Phys. Rev. C **21**, 2253 (1980).
[42] K. R. Lassey and B. H. J. McKellar, Phys. Rev. C **11**, 349 (1975).
[43] M. H. Macfarlane and J. B. French, Rev. Mod. Phys. **32**, 567 (1960).
[44] E. K. Warburton and B. A. Brown, Phys. Rev. C **46**, 923 (1992).
[45] M. Yasue, M. Tanaka, T. Hasegawa, K. Nisimura, H. Ohnuma, H. Shimizu *et al.*, Nucl. Phys. A **509**, 141 (1990).
[46] S. M. Wang, W. Nazarewicz, R. J. Charity, and L. G. Sobotka, Phys. Rev. C **99**, 054302 (2019).